Quantum Electronics **50** (6) 576–580 (2020)

https://doi.org/10.1070/QEL17339

Miniature quantum frequency standard based on the phenomenon of coherent population trapping in vapours of ^{87}Rb atoms

M.N. Skvortsov, S.M. Ignatovich, V.I. Vishnyakov, N.L. Kvashnin, I.S. Mesenzova, D.V. Brazhnikov, V.A. Vasil'ev, A.V. Taichenachev, V.I. Yudin, S.N. Bagayev, I.Yu. Blinov, V.G. Pal'chikov, Yu.S. Samokhvalov, D.A. Parekhin

Abstract. **We report the results of the development and production of a quantum frequency standard (QFS) based on the coherent population trapping (CPT) resonance observed on the D_1 absorption line of ^{87}Rb atoms. The effect of various physical factors on the QFS frequency is studied, and the optimal physical parameters of the device to attain the best frequency stability are determined. The measured relative frequency instability (Allan deviation) is $\sim 9 \times 10^{-12}$ for the averaging time of 1 s, 3×10^{-13} for 1000 s, and 1.5×10^{-12} for 24 hours. For a volume of 60 cm^3, the power consumption of the entire device is 300 mW. The designed QFS can be used in a new-generation satellite navigation systems with increased accuracy and reliability, as well as for solving a number of other problems of science and technology.**

Keywords: *quantum metrology, frequency standards, coherent population trapping, buffer gas, rubidium, radiation frequency noises, vertical-cavity surface-emitting lasers, Allan deviation.*

1. Introduction

The phenomenon of coherent population trapping (CPT), discovered in the 70s of the last century [1], finds important applications in modern science and technology. In most applications, CPT manifests itself in the form of narrow nonlinear resonances in the absorption of laser radiation when it passes through a cell filled with vapours of atoms. As the latter, alkali metals (Rb, Cs, K, and Na) are most commonly used. In the field of quantum metrology, these resonances serve as reference for oscillator frequency stabilisation in miniature quantum frequency standards (QFS's) of the microwave range (atomic clocks), and are also used for the development of certain types of scalar and vector atomic magnetometers [2–4].

The essence of the CPT phenomenon is as follows. Under the action of resonant laser radiation, a special quantum state is formed in atoms, which is a long-lived coherent superposition of magnetic sublevels of the ground state [5], where atoms do not scatter resonance radiation, resulting in a sharp decrease in its absorption in the medium. This also leads to a decrease in the fluorescence of atoms, and so in the literature such resonances are often called 'dark'. One of the most important features of dark resonances is that their width, associated with the dark state's lifetime, can be much less than the natural width of the spectral line and reach hundreds and units of Hertz when using a buffer gas [6, 7] or cells with antirelaxation coating of the walls [8, 9].

To observe dark resonances, both single-frequency and multi-frequency magneto-optical medium excitation schemes can be used. In the latter, which are commonly used in QFS's, laser radiation spectrum contains two optical frequencies (ω_1 and ω_2) being in resonance with the corresponding frequencies of dipole transitions in atoms. In the case of alkali metal atoms which only have a single electron on the outer shell, it is preferable to use the D_1 line to observe CPT resonances, since, in this case, their contrast is much higher than that when using the D_2 line [10]. In QFS's, dark resonances are observed when scanning the frequency difference ($\omega_1 - \omega_2$), and namely, when this difference becomes close to the microwave frequency of hyperfine splitting of the ground state in atom, a narrow CPT resonance is observed. Thus, using CPT resonances, it is possible to stabilise the local oscillator's microwave frequency.

The studies conducted in this work are aimed at the QFS development based on CPT resonances in a multi-frequency laser field interacting with vapours of ^{87}Rb atoms (the splitting frequency of the ground state is approximately equal to 6.83 GHz). A miniature QFS with a total volume of 60 cm^3 and an energy consumption of about 300 mW is presented and its main characteristics are investigated. In particular, the relative instability of the QFS frequency (Allan deviation) is approximately 9×10^{-12} for 1 s, 3×10^{-13} for 1000 s and 1.5×10^{-12} for 24 h. Given the totality of the demonstrated

M.N. Skvortsov, S.M. Ignatovich, N.L. Kvashnin, I.S. Mesenzova, V.A. Vasil'ev Institute of Laser Physics, Siberian Branch, Russian Academy of Sciences, prosp. Akad. Lavrent'eva 15B, 630090 Novosibirsk, Russia; e-mail: mesenzova.i@yandex.ru;
V.I. Vishnyakov Institute of Laser Physics, Siberian Branch, Russian Academy of Sciences, prosp. Akad. Lavrent'eva 15B, 630090 Novosibirsk, Russia; Novosibirsk State Technical University, prosp. K. Marksa 20, 630073 Novosibirsk, Russia;
D.V. Brazhnikov, A.V. Taichenachev, S.N. Bagayev Institute of Laser Physics, Siberian Branch, Russian Academy of Sciences, prosp. Akad. Lavrent'eva 15B, 630090 Novosibirsk, Russia; Novosibirsk State University, ul. Pirogova 1, 630090 Novosibirsk, Russia;
V.I. Yudin Institute of Laser Physics, Siberian Branch, Russian Academy of Sciences, prosp. Akad. Lavrent'eva 15B, 630090 Novosibirsk, Russia; Novosibirsk State Technical University, prosp. K. Marksa 20, 630073 Novosibirsk, Russia; Novosibirsk State University, ul. Pirogova 1, 630090 Novosibirsk, Russia;
Yu. Blinov, Yu.S. Samokhvalov, D.A. Parekhin Federal State Unitary Enterprise 'All-Russian Scientific Research Institute of Physical-Technical and Radiotechnical Measurements', 141570 Mendeleevo, Moscow region, Russia;
V.G. Palchikov Federal State Unitary Enterprise 'All-Russian Scientific Research Institute of Physical-Technical and Radiotechnical Measurements', 141570 Mendeleevo, Moscow region, Russia; National Research Nuclear University MEPhI, Kashirskoye shosse 31, 115409 Moscow, Russia

Received 11 March 2020, revision received 30 March 2020
Kvantovaya Elektronika **50** (6) 576–580 (2020)
Translated by M.A. Monastyrskiy

characteristics, the developed QFS is superior to existing commercial analogues [11, 12]. This QFS can be used in new-generation satellite navigation systems with increased accuracy of coordinate determination, as well as in other precision electronic equipment.

2. Design of a miniature QFS

The QFS functional scheme is shown in Fig. 1. A vertical-cavity surface-emitting laser (VCSEL) operates at a wavelength of 795 nm, corresponding to the D_1 line of ^{87}Rb. The laser is powered by a precision current source, and the temperature is controlled by a thermal stabilisation system. The laser output radiation is linearly polarised and passes through a quarter-wave phase plate to obtain circular polarisation. The neutral optical filter used to obtain the optimum radiation power level is located at a small angle to the laser output window to prevent back reflections to the laser. Then the radiation is passed through an absorbing cell with rubidium vapour and a buffer gas. To observe absorption in alkali metal atoms, the cell is uniformly heated above 50 °C. Due to the design features of the cell windows, they have a lower temperature, and metal condensation is observed on them. To solve this problem, the cell temperature T_c is maintained 5 °C above the temperature T_f of the finger in which the metal rubidium is located.

Helmholtz coils are located on the cell housing to produce a uniform magnetic field directed along the wave vectors of the waves. This field splits the energy levels of the ground state and allows observing the CPT resonance that is only associated with magnetic sublevels with quantum numbers $m_F = 0$, for which the linear Zeeman effect vanishes. However, these levels undergo a quadratic shift in the magnetic field, which results in a corresponding shift in the CPT resonance (frequencies of the clock 0–0 transition):

$$\Delta\omega = K_0 B^2, \tag{1}$$

where B is the magnetic field induction (in G), and, using the Breit–Rabi formula [13], it can be shown that, for ^{87}Rb atoms, the proportionality coefficient is $K_0 = 2\pi \times 575.14$ Hz $\times$ G^{-2}. The magnetic field value in our case was 100–150 mG.

To obtain the resonant optical frequencies ω_1 and ω_2 in the radiation spectrum of the laser, its current is modulated with a frequency of 3.417 GHz, supplied from a microwave oscillator. In this case, the oscillator frequency is synthesised from a frequency of 10 MHz supplied from a temperature-compensated crystal oscillator (TCXO). The frequencies ω_1 and ω_2 are side frequencies of the ±1 orders of the resulting frequency-modulated laser radiation.

An automatic control system operating at a frequency of ~15 kHz stabilises the optical frequency of laser radiation along the D1 absorption line of ^{87}Rb. To obtain an error signal, the first optical power modulation harmonic of the beam transmitted through the rubidium cell is synchronously detected. The operating frequency of the probe modulation (15 kHz) is chosen on the principle that, at this frequency, both laser and electronic components usually do not have excessive flicker noise. It is possible to control the laser generation frequency by changing the laser's supply current or temperature. The changes in current by speed are many times higher than those in the temperature method; however, with a change in current, the laser output power, impedance, and modulation characteristics change to a much greater extent. With allowance for this feature, the error signal of automatic

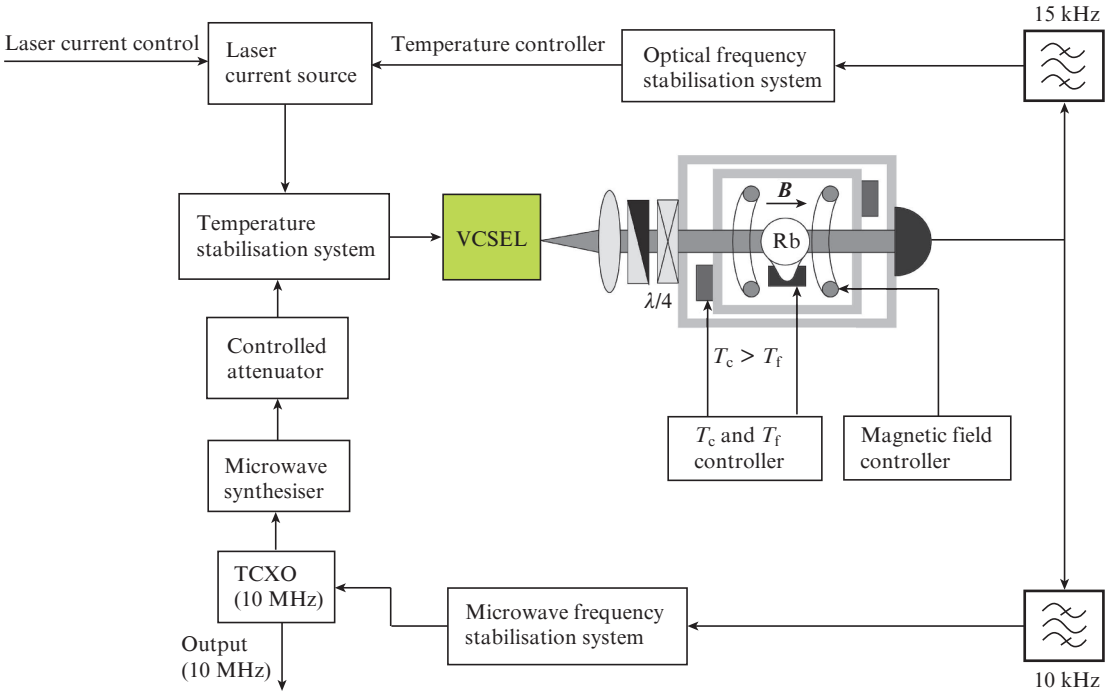

Figure 1. QFS functional scheme based on the CPT phenomenon on the D1 line of ^{87}Rb; TCXO is a temperature-compensated crystal oscillator, T_c is the cell temperature, T_f is the cell finger temperature.

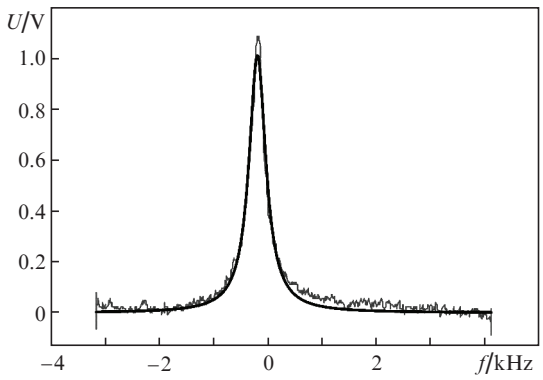

Figure 2. CPT resonance contour in ^{87}Rb atoms when scanning the microwave oscillator frequency near 3.4 GHz; U is the photodetector signal, FWHM ≈ 680 Hz.

control system is processed by adjusting the laser temperature, while the probe modulation is performed through the laser current. This approach also compensates for the error associated with inaccuracy of measuring the diode temperature by a thermal sensor.

To stabilise the microwave oscillator frequency, a stabilisation method is employed, which is similar to the Pound–Drever–Hall locking technique that is applied for laser frequency stabilisation in the optical range [14]. In this method, the modulation frequency significantly exceeds the resonance width. In our case, we use an automatic control system with a modulation frequency of ~10 kHz at full width at half maximum (FWHM) of the observed CPT resonance, equal to 680 Hz (Fig. 2). This method has a number of advantages: it allows implementation of the highest possible speed, selection of a high operating frequency to improve the signal-to-noise ratio, and also has a lock-in band up to the operating frequency.

The absorption cell is made of borosilicate glass that is resistant to alkali metals and has low gas permeability (for example, the C51-1 brand). The glass cell contains a pure ^{87}Rb isotope and an inert buffer gas (pressure ~100 Torr). In the absence of a buffer gas, the time of coherent interaction of rubidium atoms with the laser field is determined by the time-of-flight of atoms through the beam, which leads to a substantial broadening of the CPT resonances. Figure 3 shows the appearance of the cell and the quantum standard as a whole (without an external casing).

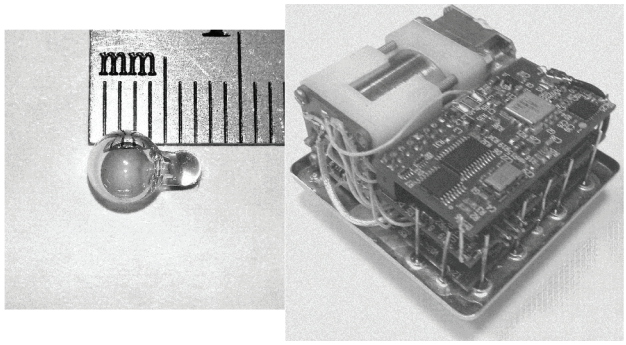

Figure 3. Absorbing cell with vapours of ^{87}Rb atoms (left) and a quantum frequency standard based on the CPT phenomenon (right).

3. Spectroscopy of CPT resonances and studying QFS characteristics

3.1. CPT resonance shift due to changes in cell temperature

To minimise the CPT resonance frequency shift and, as a consequence, the QFS output signal shift caused by a change in the cell temperature, a mixture of Ar and Ne buffer gases is used (P_{Ar}/P_{Ne} = 35/65 Torr). It is known [15, 16] that buffer gases consisting of light atoms or molecules (for example, H_2, N_2, He, Ne) lead to an increase in the 0–0 transition frequency in the rubidium atom with increasing pressure and temperature, whereas heavy buffer gases (Ar, Xe, Kr) lead to a decrease in this frequency. In addition, these dependences are nonlinear [17], and it is possible to select a mixture of buffer gases at which the dependence of the 0–0 transition frequency shift on the cell temperature has an extremum (Fig. 4). Near this extremum, the frequency shift of the 0–0 transition and, therefore, that of the CPT resonance, are not sensitive to small variations in the cell temperature. This feature enables improving the long-term QFS frequency stability. The proportion of buffer gases in our experiments allowed us to bring the extremum point in the $\Delta f(T)$ dependence into the region of 65 °C. At this temperature, the maximum signal-to-noise ratio is observed in the experiments, which is important for attaining the best short-term QFS frequency stability. The steepness of the curve in Fig. 4 is such that, at a temperature detuning by 1 °C, the relative resonance frequency shift is $\sim 5.85 \times 10^{-12}$, which can be considered an acceptable value. The temperature at which the minimum frequency shift is observed is ~64 °C.

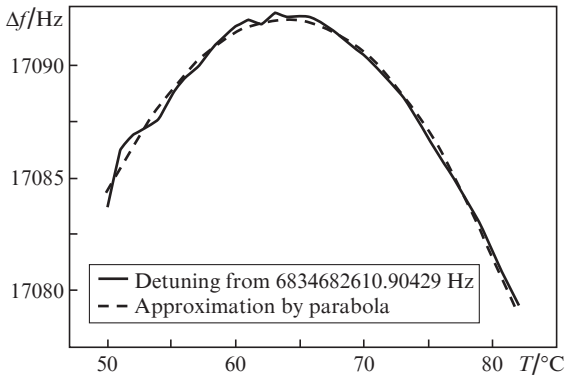

Figure 4. Dependence of the CPT resonance frequency shift on the cell temperature.

3.2. CPT resonance shift due to microwave power changes

A light shift is the shift of atomic energy levels in the presence of laser radiation, associated with the dynamic Stark effect which is quadratic in field strength (linear in intensity I). For a specific energy level in the atom, this shift is approximately proportional to the I/δ ratio and, therefore, depends not only on the optical frequency detuning δ of the light field from the transition frequency in atom, but also on its sign. In the case of a three-level Λ-scheme, the light field consisting only of two spectral components $\omega_1 > \omega_2$ with Rabi frequencies R_1 and R_2 causes a shift in the 0–0 transition frequency according to a simple expression [18]:

$$\Delta\omega = -\frac{1}{4}(R_1^2 - R_2^2)\frac{\Delta_0}{(\gamma/2)^2 + \Delta_0^2}, \quad (2)$$

where Δ_0 is the detuning of the laser field frequency from the average frequency $(\omega_1 + \omega_2)/2$ of two transitions, and γ is the total width of the spectral (optical) transition line with allowance for collisional broadening.

When using a multi-frequency laser field as in our case with a VCSEL, each of the spectral components participates in the formation of the 0–0 transition frequency shift. The approximate expression for this shift in the case of harmonic frequency modulation and γ, $\Delta_0 \ll \omega_{\rm hfs}$ can be written in the form [2, 17]:

$$\frac{\Delta\omega}{\omega_{\rm hfs}} = \left(\frac{R_0}{\omega_{\rm hfs}}\right)^2 \left[\theta(m) + \xi(m)\left(\frac{\Delta_0}{\omega_{\rm hfs}}\right)^2\right], \quad (3)$$

where $\omega_{\rm hfs}$ is the hyperfine splitting frequency (6.83 GHz in ^{87}Rb), and R_0 is the Rabi frequency which is the same for the two arms of the Λ-scheme and in the regime with no microwave modulation of the laser field. The coefficients $\theta(m)$ and $\xi(m)$ are functions of the index m of radiation frequency modulation:

$$\theta(m) = J_0^2(m) + \frac{1}{2}J_{p/2}^2(m) - 2\sum_{n=1\neq p/2}^{\infty} J_n^2(m)\frac{p^2}{(2n)^2 - p^2}, \quad (4)$$

$$\xi(m) = 4J_0^2(m) - 8\sum_{n=1\neq p/2}^{\infty} J_n^2(m)\frac{12n^2 + p^2}{[(2n)^2 - p^2]^3}p^4. \quad (5)$$

Here, J_i are the Bessel functions of the first kind of the ith order, and p is an even integer defined as the ratio of the hyperfine splitting frequency $\omega_{\rm hfs}$ to the laser modulation frequency $\omega_{\rm m}$. It should be noted that expression (3) does not take into account the asymmetry of the VCSEL optical spectrum, which often occurs due to spurious amplitude modulation (see, for example, [19–21]).

Figure 5 shows the dependence of the signal frequency at the QFS output on the microwave oscillator power when the initial power is reduced by an attenuator in the range from –16 to –1.5 dB. The VCSEL operating current was chosen equal to 1.4 mA; for this current, at the point of a minimum shift of the QFS frequency, when the microwave power is changed by 0.5 dB, the relative frequency change is $\sim 3.2 \times 10^{-12}$. Figure 5 also indicates that, as the standard's sensitivity to the microwave power level decreases, so does the sensitivity to the optical power change (this change is equivalently expressed through a change in the signal at the photodetector). Therefore, the minimum point on these dependences is the QFS operating point.

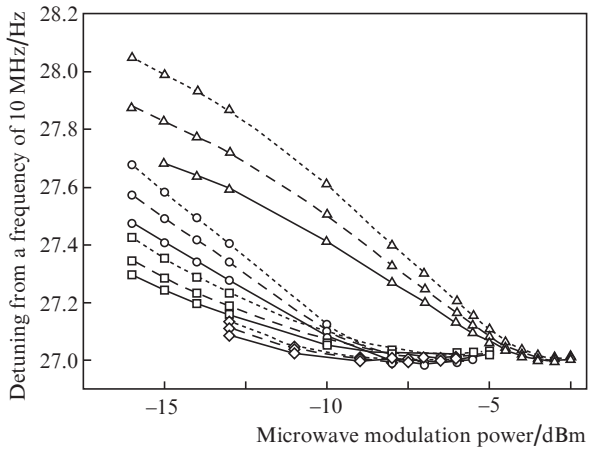

Figure 5. Dependence of the 10-MHz QFS output frequency shift on the microwave oscillator power at different intensities of the radiation registered by the photodetector (in volts), and at the laser current $I_{\rm las}$ = (□) 1.1, (◇) 1.2, (○) 1.4 and (△) 1.6 mA; U = 2 V (solid curves), 2.5 V (dashed curves), and 3 V (dotted curves).

3.3. Relative QFS frequency stability and the shift budget

With an increase in the microwave signal level, the modulation index m also increases, which causes a decrease in the intensity of the spectral components that form the CPT resonance. However, the signal-to-noise ratio does not change so significantly, which leads to a small difference in the Allan deviation during 1 s (Fig. 6). At the same time, there is a significant improvement in long-term stability due to the low sensitivity of the CPT resonance frequency shift to variations in the microwave oscillator power and the optical power of the laser (see Section 3.2).

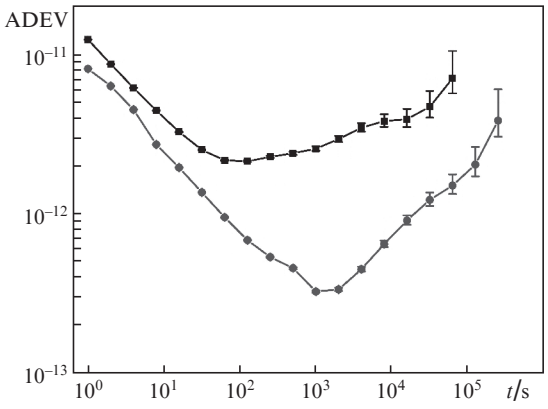

Figure 6. Allan deviation of the QFS output signal (10 MHz) (■) in the regime of measurement at the maximum CPT resonance amplitude and (●) in the regime of minimum sensitivity of the resonance shift.

Shifts and stability were measured at two different power regimes of the microwave oscillator: in the regime of maximum amplitude of the CPT resonance and in the regime of minimum sensitivity of the resonance shift to variations in the microwave oscillator power. The measurement data are given in Table 1, the contribution to daily instability is calculated as the average value for several data sets (Allan deviation is shown in Fig. 6 for one of the best QFS samples).

4. Conclusions

The work describes the developed quantum frequency standard based on the phenomenon of coherent population trapping in vapours of ^{87}Rb atoms, as well as its characteristics. In particular, the dependence of the 10 MHz QFS output signal frequency shift on the power of the microwave oscillator that modulates the laser current was studied. This dependence allowed us to determine the optimal oscillator power (the

Table 1. Budget of the QFS signal frequency shifts (10 MHz) measured at two different microwave oscillator powers.

Shift type	Stability of values in the experiment	Maximum contrast of the CPT resonance		Minimum sensitivity of the CPT resonance shift to the microwave power variations	
		Shift instability	Contribution to the daily clock instability	Shift instability	Contribution to the daily clock instability
Gas cell temperature	1 mK	0.1 mHz K^{-1}	1×10^{-14}	0.1 mHz K^{-1}	1×10^{-14}
Magnetic field of Helmholtz coil	10^{-5} G (0.1 μA)	0.1 Hz G^{-1}	1×10^{-13}	0.1 Hz G^{-1}	1×10^{-13}
Microwave modulation deviation	10^{-4} dB s^{-1} 10^{-2} dB per 24 hours	66 mHz dB^{-1}	6.6×10^{-11}	3.4 mHz dB^{-1}	3.4×10^{-12}
Optical frequency variation	100 kHz	1×10^{-6} Hz MHz^{-1}	1×10^{-14}	1×10^{-6} Hz MHz^{-1}	1×10^{-14}
Optical power variation	4 mV per 24 hours	0.045 Hz V^{-1}	1.8×10^{-11}	0.006 Hz V^{-1}	2.4×10^{-12}

index of radiation frequency modulation) at which the QFS output signal frequency is not sensitive to small variations in microwave power. It was found that at this power, the QFS signal frequency also has a weak sensitivity to variations in the optical power of laser radiation. The studies allowed us to obtain high long-term stability of the QFS signal at the level of $\sigma_y \approx 1.5 \times 10^{-12}$ per 24 h. The resulting power consumption of the entire standard is at the level of 300 mW with a total device volume of about 60 cm^3. The effect of various other physical factors on the QFS signal frequency has also been investigated. The results of these measurements are summarized in Table 1.

To compare the developed QFS with similar commercially available devices, we consider two rubidium miniature frequency standards from well-known manufacturers. In particular, the SA.35m (Microsemi) frequency standard has a short-term stability of 3×10^{-11} for 1 s, a power consumption at a level of 5 W with a volume of 50 cm^3 [12]. Another commercial product, NAC1 (AccuBeat Ltd.), has a short-term stability of 2×10^{-10} per 100 s with a power consumption of 1.2 W and a volume of 32 cm^3 [11]. Thus, the QSF we have developed is not inferior in its characteristics to commercially available analogues, and in some respects significantly exceeds them. Our QFS can find applications in a new- generation satellite navigation system with increased accuracy of coordinate determination, in communication systems with a large data flow, in astrophysics in the development of radio interferometry systems with an extra-long base and other systems where a high degree of signal synchronisation is required.

Acknowledgements. The work of the co-authors from the ILP SB RAS was performed within the framework of the State Assignment of the Ministry of Science and Higher education of the Russian Federation (Topic No. AAAA17-117030310294-3).

References

1. Alzetta A., Gozzini A., Moi L., Orriols G. *Nuovo Cimento B*, **36**, 5 (1976).
2. Vanier J. *Appl. Phys. B*, **81**, 421 (2005).
3. Kitching J. *Appl. Phys. Rev.*, **5**, 031302 (2018).
4. Guidry M.A., Kuchina E., Novikova I., Mikhailov E.E. *J. Opt. Soc. Am. B*, **34** (10), 2244 (2017).
5. Arimondo E. *Prog. Optics*, **35**, 257 (1996).
6. Brandt S., Nagel A., Wynands R., Meschede D. *Phys. Rev. A*, **56**, R1063 (1997).
7. Vanier J., Godone A., Levi F. *Phys. Rev. A*, **58**, 2345 (1998).
8. Klein M., Novikova I., Phillips D.F., Walsworth R.L. *J. Mod. Opt.*, **53**, 2583 (2006).
9. Nasyrov K., Gozzini S., Lucchesini A., Marinelli C., Gateva S., Cartaleva S., Marmugi L. *Phys. Rev. A*, **92**, 043803 (2015).
10. Stähler M., Wynands R., Knappe S., Kitching J., Hollberg L., Taichenachev A., Yudin V. *Opt. Lett.*, **27**, 1472 (2002).
11. Nano Atomic Clock 1, https://www.accubeat.com.
12. Miniature Atomic Clock SA.3Xm, https://www.microsemi.com.
13. Breit G., Rabi I.I. *Phys. Rev.*, **38**, 2082 (1931).
14. Drever R.W.P., Hall J.L., Kowalski F.V. *Appl. Phys. B*, **31** (2), 97 (1983).
15. Beaty E.C., Bender P.L., Chi A.R. *Phys. Rev. Lett.*, **1**, 311 (1958).
16. Robinson L.B. *Phys. Rev.*, **117**, 1275 (1960).
17. Bean B.L., Lambert R.H. *Phys. Rev. A*, **13**, 492 (1976).
18. Levi F., Godone A., Vanier J. *IEEE Trans. Ultrason. Ferroelectr. Freq. Control*, **47**, 466 (2000).
19. Gruet F., Al-Samaneh A., Kroemer E., Bimboes L., Miletic D., Affolderbach C., Wahl D., Boudot R., Mileti G., Michalzik R. *Opt. Express*, **21**, 5781 (2013).
20. Vas'kovskaya M.I., Vasil'ev V.V., Zibrov S.A., Yakovlev V.P., Velichansky V.L. *Tech. Phyz. Lett.*, **44**, 20 (2018) [*Pis'ma Zh. Tekh. Fiz.*, **44**, 51 (2018)].
21. Makarov A.O., Ignatovich S.M., Vishnyakov V.I., Mesenzova I.S., Brazhnikov D.V., Kvashnin N.L., Skvortsov M.N. *AIP Conf. Proc.*, **2098**, 020010 (2019).